ISSN 1052-6188, Journal of Machinery Manufacture and Reliability, 2024, Vol. 53, Suppl. 1, pp. S1–S6. © Pleiades Publishing, Ltd., 2024.
Russian Text © The Author(s), 2024, published in Problemy Mashinostroeniya i Avtomatizatsii, 2024, No. 3, pp. 4–11.

RELIABILITY, STRENGTH, AND WEAR RESISTANCE OF MACHINES AND STRUCTURES

Quantitative Phase Analysis of a Coating Based on a CrMnFeCoNiCu High-Entropy Alloy

Yu. A. Abzaev[a], A. A. Guda[b,e,*], M. S. Syrtanov[c], S. A. Guda[b,e], O. V. Kudryakov[d,e], and V. I. Kolesnikov[e]

[a] *Tomsk State University of Architecture and Construction, Tomsk, Russia*

[b] *The Smart Materials Research Institute, Southern Federal University, Rostov-on-Don, Russia*

[c] *Tomsk Polytechnic University, Tomsk, Russia*

[d] *Donskoi State Technical University, Rostov-on-Don, Russia*

[e] *Rostov State Transport University, Rostov-on-Don, Russia*

**e-mail: guda@sfedu.ru*

Received July 5, 2024; revised July 18, 2024; accepted July 25, 2024

Abstract—Films of the CrMnFeCoNiCu high-temperature alloy have been deposited onto a steel substrate by vacuum sputtering in the magnetron evaporation mode. The local atomic structure and phase composition are studied. The structural state of the CrMnFeCoNiCu alloy is determined by the superposition of contributions of equiatomic simple cubic lattices with lattice parameters of the *P*1 space group. Reflexes from the S1 and S2 phases contribute to the integral intensity; the contribution is 65.7 and 28.9%, respectively. The spatial distribution of the atoms obtained by theoretical analysis for the S1 and S2 lattices confirms that the chosen composition is a solid solution and that secondary phases are absent.

Keywords: tribological coatings, high-entropy alloys, X-ray absorption spectrometry, magnetron sputtering

DOI: 10.1134/S1052618824701164

INTRODUCTION

Unlike doped alloys based on iron, titanium, aluminum, etc., a novel class of high-entropy alloys (HEAs) has a high configuration entropy the contribution of which to the stabilization of solutions is significantly higher. HEAs are characterized by a high mixture entropy, low atomic diffusion, lattice distortions, and simple lattices (FCC, BCC, and HCP) [1, 2]. HEAs are also attractive because of their exclusive strength properties at high temperatures [3], plasticity, impact strength at cryogenic temperatures, and the combination of strength and plasticity [4, 5]. Fundamental studies of HEAs significantly broadened the number of single-phase high-entropy materials [6–8]. However, complete structural information on HEAs is limited.

HEAs based on 3*d* metals demonstrate noticeable mechanical and tribological properties. Alloys such as CoCrMnFeNi and CrMnFeCoNiCu can form microstructures with a single-phase FCC lattice [9, 10] that improves the strength of materials. The addition of copper to the CrMnFeCoNiCu system causes the formation of a Cu-enriched phase, improving the hardness and yield strength [11]. Due to the controlled cooling from the CrMnFeCoNiCu alloy melt, Cr-enriched inclusions can form in a Cr-depleted matrix that results in the formation of the $Mn_{17}Fe_{21}Co_{24}Ni_{24}Cu_{14}$ nonequiatomic composition. This modified composition and microstructure can provide better mechanical and tribological characteristics compared with the equiatomic CrMnFeCoNiCu alloy [10].

The structural composition of the coating of the six-element CrMnFeCoNiCu HEA with equimolar composition [12, 13] obtained by film deposition on a steel substrate should be studied. This study aims to identify the structural state of CrMnFeCoNiCu HEA films by X-ray diffraction. The quantitative content of phases was determined using the Rietveld method and crystallographic base of standards created using evolutionary algorithms that allow one to select the materials for the HEA coating deposition.

Table 1. Parameters of magnetron sputtering of the CuFeCoCrMnNi coating

Target composition, at %	CuFeCoCrMnNi (13.2/18.0/17.9/15.9/16.9/17.8)
Sublayer material	Cr
Method of applying the sublayer	Cathodic arc
Cathode composition for the sublayer	Cr 100%
Time of sublayer application, h	0.5
Rate of sublayer deposition, μm/min	0.02
Coating deposition time, h	5
Working pressure in the chamber during sublayer application, Pa	0.17
Working pressure in the chamber during coating application, Pa	0.82
Substrate temperature, °C	250
Bias unit voltage, V	250
Bias unit current, mA	2000
Bias unit power, W	5000
Magnetron unit voltage, V	515
Magnetron unit current, mA	2000
Magnetron unit power, W	1360
Magnetic separation of arc, no. of coil (solenoid)/current, A	c3/0; c4/1; c5/1; c6/0; c7/0;
Magnetron type	Unbalanced
Current on sources, A	120

EXPERIMENTAL

The coatings were deposited using a BRV600 vacuum installation in the magnetron evaporation mode. The structural 40CrNiMo grade steel with a sorbite structure (after hardening with high tempering) was used as a substrate. The physicomechanical properties of the steel samples were the following: hardness (H) of 2.5 GPa, elasticity modulus (E) of 200 GPa, resistance to elastic yield (H/E) of 0.0125, and resistance to plastic deformation (H^3/E^2) of 0.00039 GPa. The targets for magnetron sputtering were made using powder metallurgy (Polema, Russia) by the following route: preliminary long-term thermal and ultrasonic drying of the initial powders; intensive long-term mechanical activation of the powder mixture (grinding in planetary mills to obtain ultrafine fractions and a uniform powder composition); hot pressing of the powder blank in a metal capsule at temperatures of ≥1000°C until a "powder monolith" is obtained; and manufacturing of a magnetron target by repeated precision pressing of the blank in a stamp matrix. The target consisted of six components with similar molar ratios. An increase in the component number to six increases the mixing entropy ΔS_{mix} to ≈ 15 J/(K mol), and the entropy of the studied system is higher than that of the well-known Cantor autochthonous HEAs. The parameters of coating deposition are given in Table 1.

X-ray absorption structure (XAS) spectra of films for Cr, Mn, Fe, Co, and Ni were recorded using an R-XAS Looper X-ray absorption spectrometer (Rigaku, Japan) with the Mo cathode. The voltage and current of the tube were 16 kV and 70 mA, respectively. A Ge (311) crystal was used as a monochromator; it provided an energy resolution of ~1.3 eV at an energy of 7100 eV. An ionization chamber with an Ar atmosphere under a pressure of 300 mbar was used as a detector of the radiation intensity of the incident. To measure the film signal on the substrate, an XR-100CR semiconductor silicon drift detector (AMETEK, United States) was used to record fluorescent radiation.

The lattice energies of reference samples were calculated using density functional theory with the generalized gradient approximation (GGA). The calculations were conducted with six optimization steps using the VASP software [14, 15]. The static energy of the lattices was determined at 0 K. Electron orbitals, the distribution of single-electron density, and the ground state energy were calculated in a self-consistent mode. The wave functions of the valence electrons of the phase atoms were analyzed using the plane wave

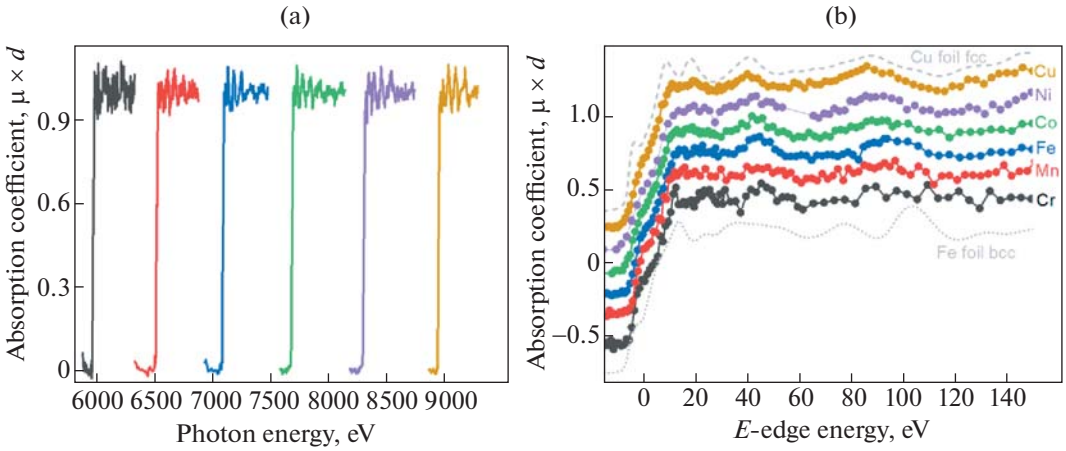

Fig. 1. (a) Normalized XAS spectra of Cr, Mn, Fe, Co, Ni, and Cu, respectively, and (b) absorption spectra of all elements on a relative energy scale in comparison with the spectra of copper and iron foils.

basis with a kinetic energy cut-off radius of 330 eV. In this case, the convergence of the total energy was ~0.5×10^{-6} eV/atom.

The X-ray diffraction study of the CrMnFeCoNiCu high-entropy alloy was carried out using an XRD-7000 diffractometer (Shimadzu, Japan) with Cu–$K\alpha$ radiation using the Bragg–Brentano parafocusing geometry. XRD patterns were collected in the 2θ range of 10°–90° with a step of 0.03 and an exposure time of 1.0 s. The voltage of an XRD tube was 40 kV, and the beam current was 30 mA. XRD data were interpreted using the unit cell library for the structure of the equiatomic CrMnFeCoNiCu composition obtained using USPEX evolutionary algorithms [16, 17].

RESULTS AND DISCUSSION

The total thickness of an intermediate layer coating was 11.28 μm, and its chemical composition was the following (wt %/at %): Ni 19.1/16.7; Fe 17.5/16.0; Co 17.1/14.9; Mn 16.5/15.4; Cr 14.0/13.8; Cu 12.4/10.0; C 2.6/11.2; O 0.7/2.1. Magnetron sputtering made it possible to increase the deposition rate of HEA metal coatings of the CuCrMnFeCoNi system by more than an order of magnitude compared with that of the cathodic arc ion plating. Magnetron sputtering of CuCrMnFeCoNi coatings was carried out at a low temperature of ~250°C. A change in the bias potential had no pronounced effect on the physicomechanical properties of the coatings. It should be mentioned that the strength of the CuCrMnFeCoNi coating is close to that of the 40CrNiMo quenched steel, but its resistance to elastic and plastic deformation is ~1.5 and ~2.5 times higher, respectively. Tribological tests were carried out at a sliding velocity v of 1 mm/s, on a friction path in radial motion along the circle L of 1.8 m, with normal force on a pin (load) $N = 5$ N. Steady-state friction was not observed, and μ values increased to 0.5–0.6 immediately at the running-in.

Figure 1 presents the normalized [18, 19] XAS spectra of elements of the CrMnFeCoNiCu high-entropy alloy. The position of the absorption edges and the shape of the spectra indicate that the oxidation state of all elements in the sample volume is equal to zero. The shape of the absorption spectra of HEA elements is similar, which shows the similarity of short-range local atomic structures. The relative angular and radial distributions near neighboring HEA atoms are also similar, and the phase is homogeneous.

Figure 1b shows the spectra of the Cu and Fe metal foils. It can be concluded that the film formed by magnetron sputtering is a single-phase equiatomic structure having a lattice in which each atom is surrounded with atoms of different types.

Reference crystal lattices of the CrMnFeCoNiCu high-entropy alloy required for structure identification are not given in crystallographic databases. The reference lattices of the CrMnFeCoNiCu alloy were predicted using evolutionary algorithms (USPEX code with VASP interface). The enthalpy was considered for the lattices of the known equatomic CrMnFeCoNiCu composition. The proportion of generations generated from random structures and due to heredity was 0.3 and 0.5, respectively; the fraction of generations obtained due to mutations was 0.2. The fraction of the current generation used to simulate the next generation was 0.6. A population of 30 atoms was considered in each simulation. A crystallographic

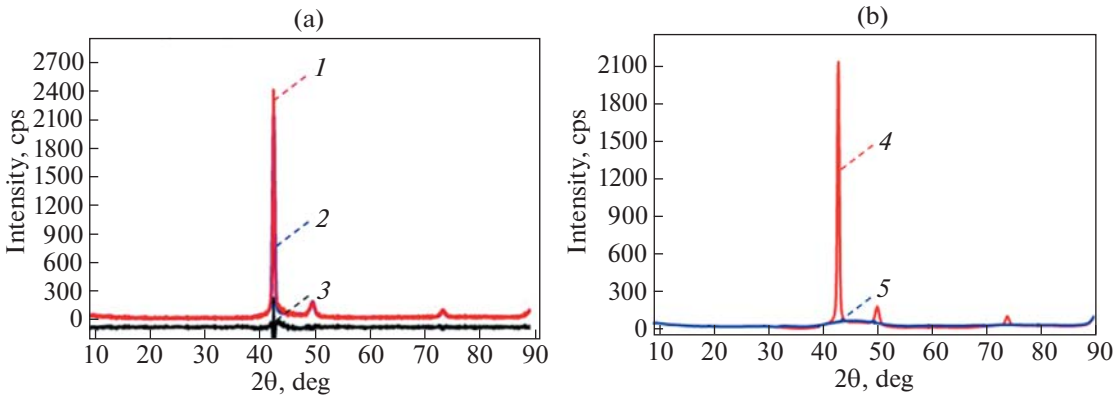

Fig. 2. XRD patterns of the CrMnFeCoNiCu alloy obtained by experiment (a) and simulation. *1,* experiment; *2,* integral intensity; *3,* intensity difference; *4,* S1; *5,* S2.

reference database was used for the quantitative Rietveld analysis. Orthorhombic lattices with close parameters were extracted from the database and converted to the *P*1 space group. The static energy and stability of these lattices against decomposition into pure components were estimated. The converted and unconverted cubic reference lattices given in the database were used for quantitative diffraction data analysis. Figure 2 presents the results of the Rietveld analysis.

The convergence of the integrated intensity to the experimental diffraction pattern was determined by the weighted profile factor ($R_{wp} \approx 3.7\%$, Table 1) and by their difference in the studied range of angles.

It was established with high reliability that the alloys with the equiatomic CrMnFeCoNiCu composition are the main phases, denoted as S1 and S2. Table 2 presents the lattice parameters, elemental composition, space group, static energy of the lattices, and phase fraction.

S1 makes the main contribution to the integration intensity; the total fraction of S1 and S2 is ≈ 0.94 (Table 2). The results show that the structure of the CrMnFeCoNiCu high-entropy alloys is determined by the superposition of these lattices. Figure 3 demonstrates the spatial distribution of atoms in the lattice of the CrMnFeCoNiCu HEA. In addition to the structure data on the reference (initial) and refined lattices given in Table 2, the atom coordinates determined by the Rietveld method are known.

According to the results obtained, the structure of the CrMnFeCoNiCu high-entropy alloy is determined by the mixture of equiatomic state lattices. It was found by the convex hull method that the CrMnFeCoNiCu alloy is stable against decomposition to intermetallides and individual elements. The decomposition energy of the CrMnFeCoNiCu HEA is $\Delta H = -0.050$ eV/atom for the following reaction:

$$CrMnFeCoNiCu \rightarrow Mn_2CrCo + Fe_5Co_3 + Fe_9Co_7 + Cr + Cu + MnNi_3.$$

This value proves that the CrMnFeCoNiCu high-entropy alloy is stable.

CONCLUSIONS

Magnetron sputtering of the high-entropy alloy was used to obtain a six-element equimolar CrMnFeCoNiCu coating. XAS spectra of all elements of the solid solution show that the valence state of all alloy elements is zero, and these elements have similar local atomic surroundings characterized by FCC

Table 2. Structural parameters of the lattices and fraction of phases of the CrMnFeCoNiCu alloy

Phase	State	*a*, Å	*b*, Å	*c*, Å	α, deg	β, deg	γ, deg	*V*, Å^3	*E*, eV	Group	Fraction, %
S1	Initial	3.623	3.623	3.623	90.0	90.0	90.0	47.54	–7828.52	1, *P*1, triclinic	65.7
	Refined	3.603	3.608	3.613	90.1	89.9	90.1	46.98	–7827.21		
S2	Initial	4.323	4.001	4.316	90.0	90.0	90.0	74.65	–7852.92	1, *P*1, triclinic	28.9
	Refined	4.156	4.329	4.318	93.6	93.4	104.2	74.95	–7850.27		

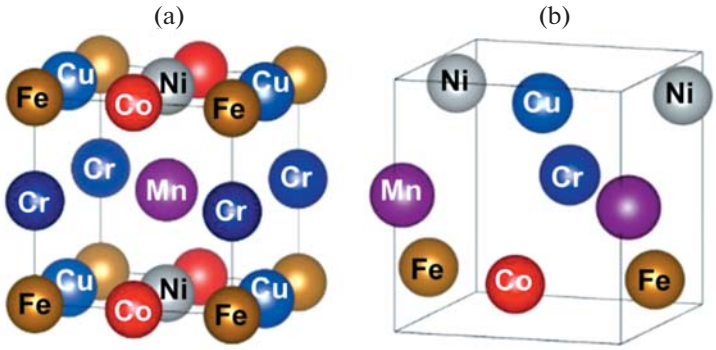

Fig. 3. Unit cells of standard lattices of the CrMnFeCoNiCu alloys (a) S1 and (b) S2 obtained by the quantitative analysis of the XRD data.

symmetry. The HEA is homogeneous and has an equiatomic element content. Using X-ray diffraction, the structural state of the CrMnFeCoNiCu coating was established to be determined by the superposition of contributions from simple cubic lattices with the space group *P*1. Rietveld analysis was used to obtain the lattice parameters and atom coordinates in unit cells. The developed analysis method and the prepared film samples will form the basis of a new-generation certified database of tribological coatings.

FUNDING

This study was supported by the Russian Science Foundation, project no. 21-79-30007.

CONFLICT OF INTEREST

The authors of this work declare that they have no conflicts of interest.

REFERENCES

1. Cantor, B., Chang, I.T.H., Knight, P., and Vincent, A.J.B., Microstructural development in equiatomic multicomponent alloys, *Mater. Sci. Eng., A*, 2004, vols. 375–377, pp. 213–218. https://doi.org/10.1016/j.msea.2003.10.257
2. Sahlberg, M., Karlsson, D., Zlotea, C., and Jansson, U., Superior hydrogen storage in high entropy alloys, *Sci. Rep.*, 2006, vol. 6, no. 1, p. 36770. https://doi.org/10.1038/srep36770
3. Senkov, O.N., Wilks, G.B., Scott, J.M., and Miracle, D.B., Mechanical properties of Nb25Mo25Ta25W25 and V20Nb20Mo20Ta20W20 refractory high entropy alloys, *Intermetallics*, 2011, vol. 19, no. 5, pp. 698–706. https://doi.org/10.1016/j.intermet.2011.01.004
4. Li, Zh., Pradeep, K.G., Deng, Yu., Raabe, D., and Tasan, C.C., Metastable high-entropy dual-phase alloys overcome the strength–ductility trade-off, *Nature*, 2016, vol. 534, no. 7606, pp. 227–230. https://doi.org/10.1038/nature17981
5. Li, X., Liang, X., Liu, D., Chen, R., Huang, F., Wang, R., Rettenmayr, M., Su, Ya., Guo, J., and Fu, H., Design of $(Nb, Mo)_{40}Ti_{30}Ni_{30}$ alloy membranes for combined enhancement of hydrogen permeability and embrittlement resistance, *Sci. Rep.*, 2017, vol. 7, no. 1, p. 209. https://doi.org/10.1038/s41598-017-00335-0
6. Li, R., Xie, L., Wang, W.Yi., Liaw, P.K., and Zhang, Yo., High-throughput calculations for high-entropy alloys: A brief review, *Front. Mater.*, 2020, vol. 7, p. 290. https://doi.org/10.3389/fmats.2020.00290
7. Lee, K., Ayyasamy, M.V., Delsa, P., Hartnett, T.Q., and Balachandran, P.V., Phase classification of multi-principal element alloys via interpretable machine learning, *npj Comput. Mater.*, 2022, vol. 8, no. 1, p. 25. https://doi.org/10.1038/s41524-022-00704-y
8. Rajendrachari, Sh., An overview of high-entropy alloys prepared by mechanical alloying followed by the characterization of their microstructure and various properties, *Alloys*, 2022, vol. 1, no. 2, pp. 116–132. https://doi.org/10.3390/alloys1020008
9. Gromov, V.E., Konovalov, S.V., Shlyarova, Yu.A., Efimov, M.O., and Panchenko, I.A., Control of Cantor CoCrFeMnNi high-entropy alloy mechanical properties, *Izv. Vyssh. Uchebn. Zaved., Chern. Metall.*, 2022, vol. 65, no. 8, pp. 563–572.

10. Ter-Isahakyan, A. and Balk, T.J., Evaluation of equiatomic CrMnFeCoNiCu system and subsequent derivation of a non-equiatomic MnFeCoNiCu alloy, *Materials*, 2023, vol. 16, no. 6, p. 2455. https://doi.org/10.3390/ma16062455
11. Xian, X., Lin, L., Zhong, Zh., Zhang, Ch., Chen, Ch., Song, K., Cheng, J., and Wu, Yu., Precipitation and its strengthening of Cu-rich phase in $CrMnFeCoNiCu_x$ high-entropy alloys, *Mater. Sci. Eng., A*, 2018, vol. 713, pp. 134–140. https://doi.org/10.1016/j.msea.2017.12.060
12. Kwon, Y.-S., Gerasimov, K.B., and Yoon, S.-K., Ball temperatures during mechanical alloying in planetary mills, *J. Alloys Compd.*, 2002, vol. 346, nos. 1–2, pp. 276–281. https://doi.org/10.1016/s0925-8388(02)00512-1
13. Hadjiafxenti, A., Gunduz, I.E., Kyratsi, T., Doumanidis, C.C., and Rebholz, C., Exothermic reaction characteristics of continuously ball-milled Al/Ni powder compacts, *Vacuum*, 2013, vol. 96, pp. 73–78. https://doi.org/10.1016/j.vacuum.2013.03.004
14. Kresse, G. and Hafner, J., Ab initio molecular dynamics for liquid metals, *Phys. Rev. B*, 1993, vol. 47, pp. 558–561. https://doi.org/10.1103/PhysRevB.47.558
15. Kresse, G. and Joubert, D., From ultrasoft pseudopotentials to the projector augmented-wave method, *Phys. Rev. B*, 1999, vol. 59, no. 3, pp. 1758–1775. https://doi.org/10.1103/physrevb.59.1758
16. Oganov, A.R. and Glass, C.W., Crystal structure prediction using ab initio evolutionary techniques: Principles and applications, *J. Chem. Phys.*, 2006, vol. 124, no. 24, p. 244704. https://doi.org/10.1063/1.2210932
17. Oganov, A.R., Lyakhov, A.O., and Valle, M., How evolutionary crystal structure prediction works–and why, *Acc. Chem. Res.*, 2011, vol. 44, no. 3, pp. 227–237. https://doi.org/10.1021/ar1001318
18. Ravel, B. and Newville, M., ATHENA and ARTEMIS interactive graphical data analysis using IFEFFIT, *Phys. Scr.*, 2005, vol. 115, p. 1007. https://doi.org/10.1238/physica.topical.115a01007
19. Newville, M., *IFEFFIT*: Interactive XAFS analysis and *FEFF* fitting, *J. Synchrotron Radiat.*, 2001, vol. 8, no. 2, pp. 322–324. https://doi.org/10.1107/s0909049500016964

Translated by N. Saetova